bioengineering

MDPI

Article

RETRACTED: Mycosynthesis of Hematite (α-Fe_2O_3) Nanoparticles Using *Aspergillus niger* and Their Antimicrobial and Photocatalytic Activities

Ebrahim Saied [1,*], Salem S. Salem [1], Abdulaziz A. Al-Askar [2,*], Fathy M. Elkady [3], Amr A. Arishi [4] and Amr H. Hashem [1,*]

1 Botany and Microbiology Department, Faculty of Science, Al-Azhar University, Nasr City 11884, Egypt
2 Department of Botany and Microbiology, Faculty of Science, King Saud University, Riyadh 12372, Saudi Arabia
3 Microbiology and Immunology Department, Faculty of Pharmacy (Boys), Al-Azhar University, Nasr City 11884, Egypt
4 School of Molecular Sciences, The University of Western Australia, Perth, WA 6009, Australia
* Correspondence: hema_almassry2000@azhar.edu.eg (E.S.); aalaskara@ksu.edu.sa (A.A.A.-A.); amr.hosny86@azhar.edu.eg (A.H.H.)

Abstract: Nanoparticles (NPs) and nanomaterials (NMs) are now widely used in a variety of applications, including medicine, solar energy, drug delivery, water treatment, and pollution detection. Hematite (α-Fe_2O_3) nanoparticles (Hem-NPs) were manufactured in this work by utilizing a cost-effective and ecofriendly approach that included a biomass filtrate of *A. niger* AH1 as a bio-reducer. The structural and optical properties of Hem-NPs were investigated using X-ray diffraction (XRD), transmission electron microscopy (TEM), dynamic light scattering (DLS), and UV-visible and Fourier-transform infrared (FTIR) spectroscopies. The results revealed that all of the studied parameters, as well as their interactions, had a significant impact on the crystallite size. The average diameter size of the biosynthesized Hem-NPs ranged between 60 and 80 nm. The antimicrobial and photocatalytic activities of Hem-NPs were investigated. The antimicrobial results of Hem-NPs revealed that Hem-NPs exhibited antibacterial activity against *E. coli*, *B. subtilis*, and *S. mutans* with MICs of 125, 31.25, and 15.62 µg/mL, respectively. Moreover, Hem-NPs exhibited antifungal activity against *C. albicans* and *A. fumigatus*, where the MICs were 2000 and 62.5 µg/mL, respectively. The efficiency of biosynthesized Hem-NPs was determined for the rapid biodegradation of crystal violet (CV) dye, reaching up to 97 percent after 150 min. Furthermore, Hem-NPs were successfully used more than once for biodegradation and that was regarded as its efficacy. In conclusion, Hem-NPs were successfully biosynthesized using *A. niger* AH1 and demonstrated both antimicrobial activity and photocatalytic activity against CV dye.

Keywords: hematite (α-Fe_2O_3); iron oxide nanoparticles; antimicrobial activity; photocatalytic activity

check for updates

Citation: Saied, E.; Salem, S.S.; Al-Askar, A.A.; Elkady, F.M.; Arishi, A.A.; Hashem, A.H. RETRACTED: Mycosynthesis of Hematite (α-Fe_2O_3) Nanoparticles Using *Aspergillus niger* and Their Antimicrobial and Photocatalytic Activities. *Bioengineering* **2022**, *9*, 397. https://doi.org/10.3390/bioengineering9080397

Academic Editors: Hirak Patra and Suryyani Deb

Received: 1 July 2022
Accepted: 10 August 2022
Published: 17 August 2022
Retracted: 22 January 2025

Publisher's Note: MDPI stays neutral with regard to jurisdictional claims in published maps and institutional affiliations.

Copyright: © 2022 by the authors. Licensee MDPI, Basel, Switzerland. This article is an open access article distributed under the terms and conditions of the Creative Commons Attribution (CC BY) license (https://creativecommons.org/licenses/by/4.0/).

1. Introduction

The textile, leather, paper, plastic, printing, culinary, and cosmetic industries all employ a variety of dyes [1]. Furthermore, dye effluents are the pollutants that are most frequently found in wastewater due to their great observability, even at trace quantities [2]. Additionally, trace dyes are extremely resistant to biodegradation by natural flora and may result in allergic dermatitis or skin irritation [3]. Many dyes are toxic, carcinogenic, or mutagenic. As a result, dye removal from wastewater is important for environmental health [4,5]. Adsorption was found to be superior to alternative wastewater treatment methods because of its low cost, adaptability, simplicity, ease of application, and lack of sensitivity to harmful substances [6]. Zeolites, activated carbons, industrial byproducts, agricultural wastes, clays, biomass, and polymeric materials have all been used to make dye

This paper has been retracted. A retraction notice was published on 22 January 2025 in *Bioengineering* **2025**, *12*, 100. https://doi.org/10.3390/bioengineering12020100

RETRACTED

adsorbents. However, these adsorbents have limited adsorption capacities and separation efficiencies limit their application [7,8]. Rapid advances in science and technology are making it possible for the development of greener nanotechnology [9,10]. Nanotechnology is characterized by the assembly and structure of nanoparticles (NPs) to manage their size [11,12]. When compared with bulk material, nanoscale material exhibits unique features. As the domains of nanotechnology have developed, their usage in the creation of microelectronics, lithium batteries, non-linear optical systems, transistors, emitting diodes, sensors, and solar energy harvesting devices has risen [10]. In medicine, nanoparticles have been used to treat cancer and to produce antimicrobial agents [13–20]. They are also utilized as catalysts in pollution control, wastewater treatment, and a variety of other applications [21]. Iron oxide NPs are regarded as outstanding materials for environmental and medicinal applications because of their low band gaps, chemical consistency, magnetic properties, and other characteristics [22]. Iron oxides offer a variety of polymorphs, including crystalline Fe_2O_3 (hematite), γFe_2O_3 (maghemite), and Fe_3O_4 (magnetite). Other forms that generally exist at high pressure are amorphous [23]. Meanwhile, hematite is an economical, abundant, and non-toxic biological source with a small size and a large surface area in the formation of α-Fe_2O_3 NPs and Fe_3O_4 NPs. The ferric oxide known as iron oxide, which is sometimes referred to as Fe_2O_3, is a common substance in nature. Under ordinary pressure and temperature conditions, it is one of the most thermodynamically stable substances. Iron oxide nanoparticles have been generated chemically and physically, such as the polyol technique [24], co-precipitation [25], sol-gel method [26], electrochemical synthesis [27], chemical vapor deposition [28], microwave irradiation [29], and pulsed laser method [30], but the drawbacks of these techniques include the requirements for highly toxic reactions with agents that reduce materials, such as sodium hydrazine and borohydride. Furthermore, these interactions may have a number of negative effects on humans and other biological systems [31]. In the past ten years, researchers have created eco-friendly NP synthesis techniques, including biosynthesis, or green synthesis. The advantages of biosynthesis processes are their simplicity, cleanliness, and environmental protection. In this aspect, fungi are particularly appealing since they are nontoxic, fast-acting, and generate large quantities of NPs [32]. Various forms of contaminants in the environment, including dyes, may be removed using NPs for environmental remediation, which are progressively damaging aquatic ecosystems by changing water chemistry. NPs have been demonstrated to have the ability to eliminate pollutants. For instance, Nagajyothi et al. [33] created metal and metal oxide NPs to degrade dyes. Iron nanoparticles were created by Goutam et al. [34] and used to reduce pollution. According to earlier research, synthesis variables including pre-cursor concentration, pH, reaction time, and temperature have an impact on nanoparticles' crystallites development [35]. This made it possible to control the crystallite size of nanoparticles by adjusting the synthesis parameters. In this investigation, novelty NP would be a cost-effective, biosynthesized green solution for antimicrobial and cleaning contaminated water. Biomass filtrate of *A. niger* AH1 was used to biosynthesize ecofriendly Hem-NPs. Different analysis were used to describe the manufactured Hem-NPs. Then, both the synthetic Hem-NPs' antibacterial and antifungal properties were investigated. Hem-NPs were examined for environmental use to determine their efficacy for the biodegradation of crystal violet (CV).

2. Materials and Methods

All the chemicals, media, reagents, and $FeSO_4 \cdot 7H_2O$ were purchased from Sigma Aldrich, Cairo, Egypt. $FeSO_4 \cdot 7H_2O$ was used as a precursor for the preparation of α-Fe_2O_3 NPs. All biological reactions were done using deionized and sterilized H_2O.

2.1. Fungus Used

Hem-NPs were myco-synthesized using a biomass filtrate of *A. niger* AH1, which was previously isolated, morphologically and genetically identified, and deposited in a gene bank with accession number MW680847 in our previous work [36].

RETRACTED

2.2. Synthesis of Hem-NPs Using a Biomass Filtrate of A. niger AH1

A. niger AH1 was inoculated in two discs (0.8 mm in diameter) and cultured in a potato dextrose broth medium for 5.0 days at 28 °C ± 2 °C with the pH adjusted to 7.0 and under shaking conditions (150 rpm). After the incubation period, the collected biomass (15 g) was rinsed (three times) with deionized and sterilized H_2O. Then, the rinsed biomass was reconstituted in 100 mL of distilled water at 30 °C ± 2 °C and shaken at 150 rpm for two days, followed by centrifugation of the suspended biomass to obtain the fungal biomass filtrate, which was utilized for the production of Hem-NPs as follows: for 24 h in the dark at 30 °C ± 2 °C with shaking at 150 rpm and the pH adjusted to 9, 100 mL of the fungal biomass filtrate was combined with 1.0 mM of $FeSO_4 \cdot 7H_2O$ (as a metal oxide nanoparticle precursor). A reddish brown color formed in the filtrate, which was collected afterward to oven-dry at 150 °C for 24 h [37]. The FBF without a metal precursor and $FeSO_4 \cdot 7H_2O$ solution were used in the experiment as controls.

2.3. Effect of Some Physic-Chemical Parameters on Hem-NPs Biosynthesis

The experiments were conducted in three replicates and the results were monitored using a UV-Visible spectrophotometer.

2.4. Effect of Incubation Times on the Biomass Filtrate and its Precursor

Incubation time plays an important role in Hem-NP production; therefore, the experiment was designed to have different time intervals (6, 12, 24, 36, 48, and 72 h) to select the best incubation time for the given high yield productivity of Hem-NPs. Using a UV-visible spectrophotometer and the color change, the ideal incubation duration was determined and measured.

2.5. Effect of pH Values on the Biomass Filtrate and its Precursor

The experiments were run with pH values of 6, 7, 8, 9, and 10 to determine the optimal pH for increasing Hem-NP production. The optimal pH was evaluated as previously described, using hydrochloric acid to adjust the pH < 7 and sodium hydroxide to adjust the pH > 7.

2.6. Effect of $FeSO_4 \cdot 7H_2O$ Concentrations

To find the ideal $FeSO_4 \cdot 7H_2O$ concentration in the reaction solutions to achieve the desired result, the experiment's design examined $FeSO_4 \cdot 7H_2O$ at four different concentrations (1 mM, 2 mM, 3 mM, and 4 mM) in the reaction solutions. The UV-Visible spectrophotometer change (Jenway 6305 Spectrophotometer) was used to detect the optimal concentration based on the color.

2.7. Purification of Biosynthesized Hem-NPs

Hem-NPs colloids were centrifuged at 10,000 rpm for 15 min after optimizing the synthesis conditions. The supernatant was discarded and the pellet, after washing, was dried at 40 °C for 48 h. The final product was collected and stored for analysis [38].

2.8. Characterization of the Optimized Hem-NPs

The biosynthesized Hem-NPs obtained under the optimal conditions were characterized using a UV-visible spectrophotometer (scanning spectra range from 350 to 750 nm using a Jenway 6305 Spectrophotometer (Jenway, Staffordshire, UK)). TEM (JEOL 1010, Tokyo, Japan) was used to examine the NP sizes and shapes. The Hem-NPs solution was drop-coated onto a copper grid that had been coated with carbon before being placed in a specimen holder to create the samples [39]. XRD patterns were used to further analyze the crystallinity of the biosynthesized Hem-NPs using an X'Pert Pro Xray diffractometer (Philips, Eindhoven, The Netherlands). The 2θ was in the range of 4° to 80°.

RETRACTED

The Debye–Scherrer equation was used to calculate the average size of the NPs biosynthesized from fungal metabolites [40].

$$D = K\lambda/\beta Cos\theta \quad (1)$$

where D stands for the average particle size, K stands for the Scherrer's constant = 0.9, λ stands for the wavelength, β stands for the maximum intensity, and θ signifies Bragg's angle. The sizes and distribution of the bio-synthesized metal oxide NPs in the colloidal fluids were examined using DLS analysis. To measure the materials with a Nano ZS Zeta Sizer (Malvern, UK), the components were dissolved in distilled water. Finally, using Fourier-transform infrared (FTIR) spectroscopy (Perkin-Elmer FTIR-1600, Waltham, MA, USA), the contributions of fungal metabolites and the various functional groups responsible for reducing, capping, and stabilizing the Hem-NPs were assessed. The FTIR spectra were scanned between 400 and 4000 cm^{-1} [41].

2.9. Antimicrobial Activity

The antimicrobial activity of biosynthesized Hem-NPs against various bacterial strains, such as Escherichia coli ATCC 25922, Pseudomonas aeruginosa ATCC 27853, Staphylococcus mutans ATCC 25175, and Bacillus subtilis ATCC605, as well as unicellular fungal strains (Candida albicans ATCC90028, *A. fumigatus* ATCC 204305) were tested using the agar well diffusion technique. The diffusion test in agar was carried out in line with Clinical Laboratory Standard Institute document M51-A2 [42] with a few minor adjustments. The bacterial strains were cultivated for 24 h at 37 °C on a nutrient agar medium. Bacterial suspensions containing 1.5×10^6 CFU/mL were aseptically poured onto sterile Petri plates after being seeded over Mueller–Hinton agar medium. Then, 100 µL of Hem-NPs (4000 µg/mL), the biomass filtrate (BF), and standard antibiotic (cefuroxime) were added to the agar well, and then the plates were put in the refrigerator for 2 h, followed by incubation at 37 °C for 24 h. On the other hand, fungal strains were initially grown on PDA plates and incubated at 30 °C for 3–5 days. The spore suspension was created in a sterile phosphate buffer solution (PBS), pH 7.0, and after being counted in a cell counter chamber, the inoculums were adjusted to 10^7 spores/mL. Agar PDA plates were evenly dispersed with 1 mL each. In order to create a well in the infected PDA plates, a sterile cork borer (7 mm) was utilized. Subsequently, 100 L of Hem-NPs (4000 µg/mL), the BF, and the reference antifungal (Nystatin) were added. The inhibition zone diameter on each PDA plate was evaluated after 72 h of 72 °C incubation. To determine the minimum inhibitory concentration, Hem-NPs were prepared in different concentrations ranging from 4000 to 3.9 µg/mL, then assessed separately to detect the MIC against selected bacterial and fungal strains [14,43,44].

2.10. Photocatalytic Degradation of Crystal Violet Dye Using Hem-NPs

To evaluate the photocatalytic efficiency of biosynthesized Hem-NPs under sunlight stimulation, the degradation of crystal violet dye was observed at various Hem-NPs concentrations (0.25, 0.5, 0.75, and 1.0 mg mL^{-1}) and for variable contact times (30.0, 60.0, 90.0, 120.0, 150.0, 180.0, and 210.0 min). To achieve the absorption/desorption equilibrium, 100 mL of the dye solutions with the desired NP content were constantly swirled for 30 min prior to the photocatalytic experiment. Another part of the experiment, consisting of the same reactions, was conducted in the dark for a comparative study. The decolorization efficacy was estimated as the following: 1.0 mL from each treatment was withdrawn and centrifuged at 10,000 rpm for 3.0 min and their optical density (O.D.) was measured at the maximum absorption band (λ_{max}) of crystal violet dye solution, i.e., 588 nm, using a spectrophotometer (721 spectrophotometers, M-ETCAL). The following formula was used to calculate the crystal violet dye's decolorization percentage (%) [45]. D (%) = [dye (i) − dye (f)/dye (i)] × 100, where D (%) is the decolorization percentage, dye (i) is the initial absorbance, and dye (f) is the final absorbance.

RETRACTED

2.11. Statistical Analysis

All results presented are the means of three independent replicates. Data were subjected to statistical analysis using the SPSS v18 (Version 18.0. SPSS Inc., Chicago, IL, USA) statistical package. The study of the mean difference between the treatments was performed using a *t*-test or analysis of variance (ANOVA), followed by Tukey's HSD test at $p < 0.05$.

3. Result and Discussion

3.1. Green Synthesis of Hematite Nanoparticles (Hem-NPs)

Aspergilli have the ability to synthesize various NPs [36]. The biomass filtrate of the fungus strain *A. niger* AH1 was used in this investigation as a catalyst to form Hem-NPs which enhance the production process, decrease the aggregation, and produce a smaller size [33]. The first observation for the biosynthesis of NPs was the changing colour of the biomass filtrate once it was mixed with metal precursors, as shown in Figure 1. Therefore, the manifestation of a reddish-brown colour after mixing the biomass filtrate with $FeSO_4{\cdot}7H_2O$ indicates the successful formation of Hem-NPs. In order to successfully biofabricate of iron oxide nanoparticles, Chatterjee et al. [46] used the manglicolous fungus Aspergillus niger BSC-1. By using a strain of Penicillium expansum, [41] created α-Fe_2O_3 NPs (Kw). Furthermore, Srivastava et al. [47] reported that Fe_3O_4/Fe_2O_3 nanocomposite was biosynthesized by using the waste pulp of Syzygium cumini [48]. Biosynthesized magnesium oxide nanoparticles were created using Penicillium chrysogenum. Mohamed et al. [49] used Penicillium chrysogenum MF318506 to prepare of ZnO and CuO nanoparticles. Mahanty et al. [50] synthesized Fe_2O_3 NPs by three strains of fungus, i.e., Fusarium incarnatum, Phialemoniopsis ocularis, and Trichoderma asperellum, were mixed with the salt solution of $FeCl_3$ and $FeCl_2$ (2:1 mM).

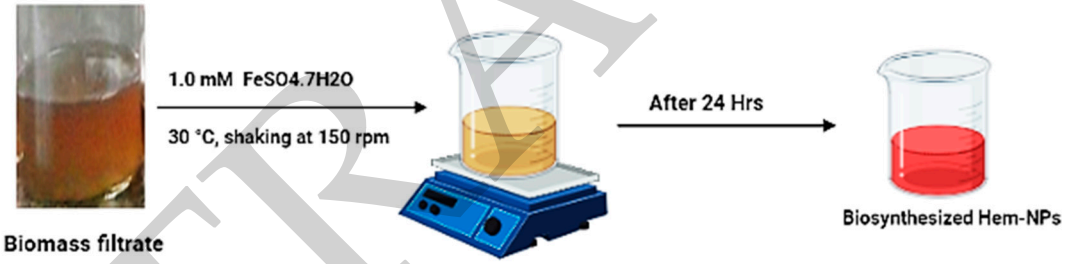


Figure 1. Biosynthesis of Hem-NPs using the biomass filtrate of *A. niger* AH1.

3.2. Factors That Affected the Hem-NP Biosynthesis

The optimal physicochemical parameters for high-yielding Hem-NPs were studied, as represented in Figure 2A–C. Hence, factors that affected Hem-NPs biosynthesis were studied, such as the incubation time in the biomass filtrate and precursor, pH values, and concentration of the precursor. The results revealed that the maximum high-yielding capacity of Hem-NPs occurred at 3 mM of ferrous sulfate heptahydrate at pH 9 after 36 h. In addition, the presence of a substrate in the medium may also induce the release of enzymes. Moreover, high ferrous salt concentrations can result in aggregated NPs of a larger size. Pallela et al. [51] used Sida cordifolia plant extract and iron nitrate as a precursor to produce deep red Hem-NPs after 8 h. Alagiri, Hamid [52] succeeded in the biosynthesis of Hem-NPs after 24 h of incubation in a tea extract and an iron nitrate solution. Alternatively, [53] made Hem-NPs by combining G. resinifera extract with $FeCl_3{\cdot}6H_2O$ (0.4 mM) and adding sodium acetate (2 M) for 2 h at 80 °C. Moreover, Vinayagam et al. [54] reported that the optimal pH was 11 for the biosynthesis of magnetic SD-Fe_2O_3 nanoparticles when using a Spondias dulcis leaf extract (SDLE). The production of iron oxide by a Penicillium expansum strain (Kw) was carried out using 1.0 mM of $FeCl_3{\cdot}6H_2O$ at pH 10.0, according to Fouda et al. [55]. In order to create (iron oxide NPs), Abbas et al. [56] combined a 0.2 M ferric chloride solution with S. platensis extract in a 1:1 volume ratio (with a final concentration of 0.1 M).

RETRACTED

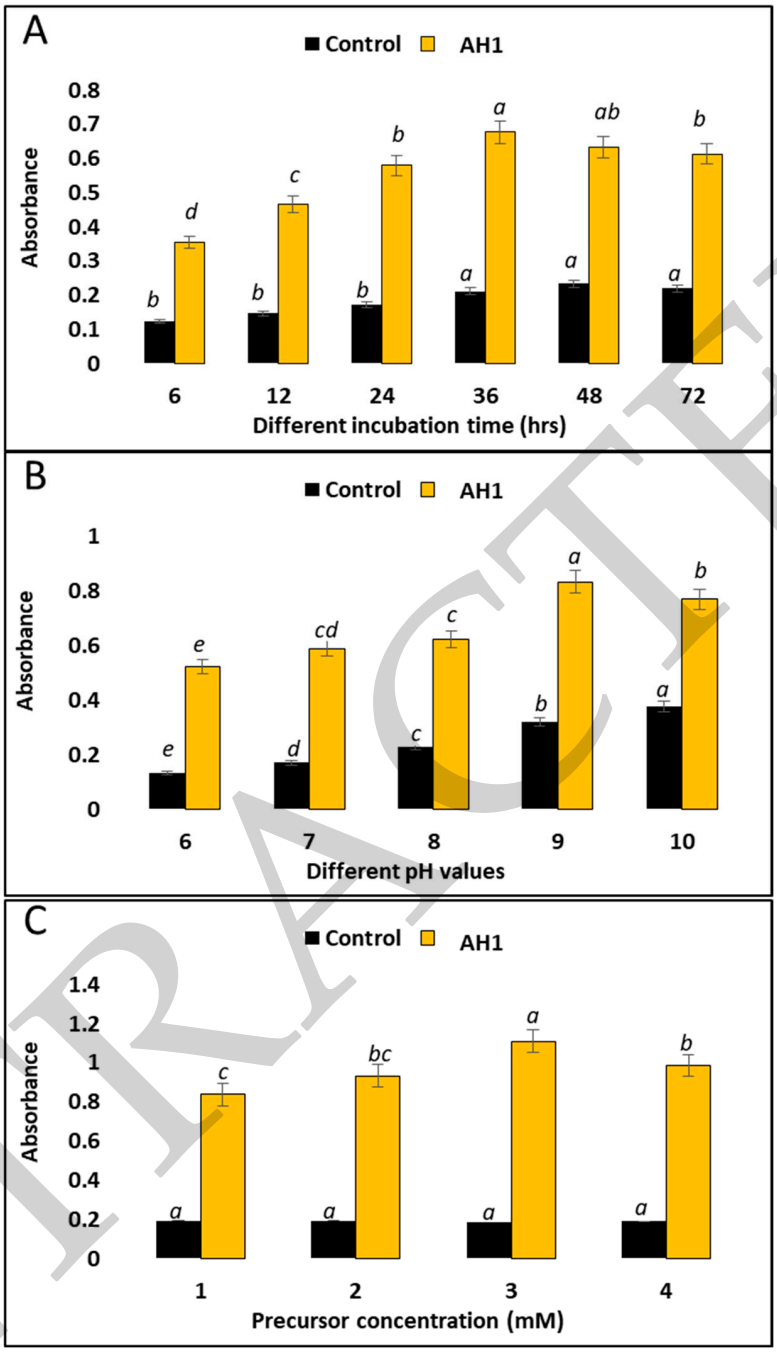


Figure 2. Optimizing factors for biosynthesized Hem-NPs using *A. niger* AH1: (**A**) the effect of the contact time between the biomass filtrate and 1.0 mM of $FeSO_4 \cdot 7H_2O$ concentration, (**B**) the effect of different pH values, and (**C**) the effect of different $FeSO_4 \cdot 7H_2O$ concentrations. Small letters a, b, c, d, ab, bc, cd show the power of significance.

3.3. Characterization of Biosynthesized α-Fe_2O_3 Nanoparticles

3.3.1. UV-Visible Spectroscopy

The colloidal solution of Hem-NPs was analyzed using UV-Visible spectroscopy. Consequently, a peak was obtained at 490 nm, as appears in Figure 3. This behavior may be attributed to the intrinsic band gap absorption of α-Fe_2O_3 due to the electron transitions from the valence band to the conduction band, where several factors, including particle size and shape, are responsible for the broadening of the peak [57,58]. According to Ahmed et al. [59] the Hem-NPs displayed broad absorption peaks in the 300–550 nm wavelength range. Asoufi et al. [60] showed an absorption band edges in the UV region at

RETRACTED

450 nm indicated the synthesized Fe_2O_3 nanoparticles by using Ailanthus excelsa leaves extract. The spectra of green iron oxide NPs was showed absorbance at 350 nm by using Leaves of P. orientalis [61]. Hem-NPs were fabricated by Tragacanth Gel has a broad peak between 200–300 nm centered at 262 nm [62]. The inconsistency in these results might be due to a particle size variance. It is well founded that the SPR bands are very susceptible and highly dependent on the nanoparticles size, shape, $FeSO_4{\cdot}7H_2O$ concentration and the type of substrates presented in the biological extract [63].

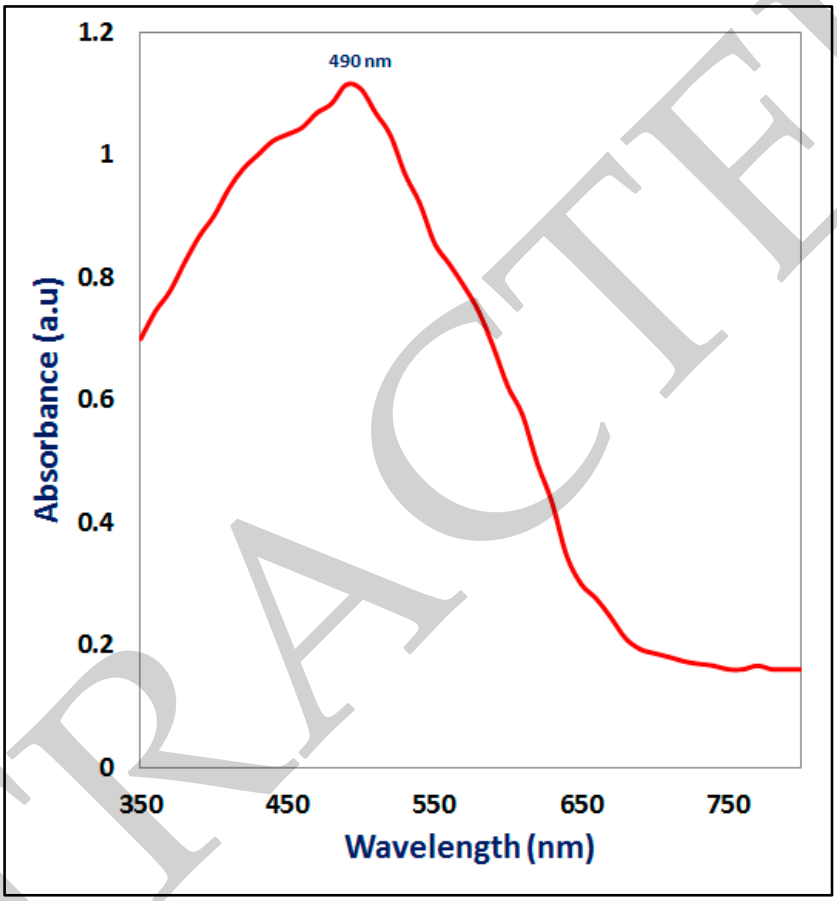


Figure 3. UV–vis spectra of Hem-NPs.

3.3.2. Fourier-Transform Infrared (FTIR) Spectroscopy

The probable availability of reducing and stabilizing biomaterials in the fungal biomass extract was determined using FTIR analysis. The resultant FTIR spectrum had several absorption bands that matched the functional groups of the biomolecules found in the fungal biomass extract (Figure 4A). The absorption peaks centered at 3755, 3377, 2928, 2429, 1620, 1384, 1076, and 1027 cm^{-1} were assigned to O–H stretching vibrations, C=O stretching vibrations [64], C=C stretching vibrations, C–O stretching vibrations [65], and the bending vibration of C-OH [66]. The peaks observed at 2928 cm^{-1} and 2429 cm^{-1} represented, respectively, the C-H asymmetric and symmetric stretching vibrations of the methyl group [67]. In addition, a peak that appeared at 1620 cm^{-1} could refer to the C–N stretching vibration band of amines. The bands observed at 1384, 1076, and 1027 cm^{-1} could be attributed to aromatic and aliphatic amine C-N stretching vibrations [55]. Furthermore, the 534 cm^{-1} peak corresponded to the Fe-O stretching vibrations [68,69]. Peaks in the 500–1000 cm^{-1} wavelength range were mostly caused by metal–oxygen group bonding, confirming the production of α-Fe_2O_3 NPs [70].

RETRACTED

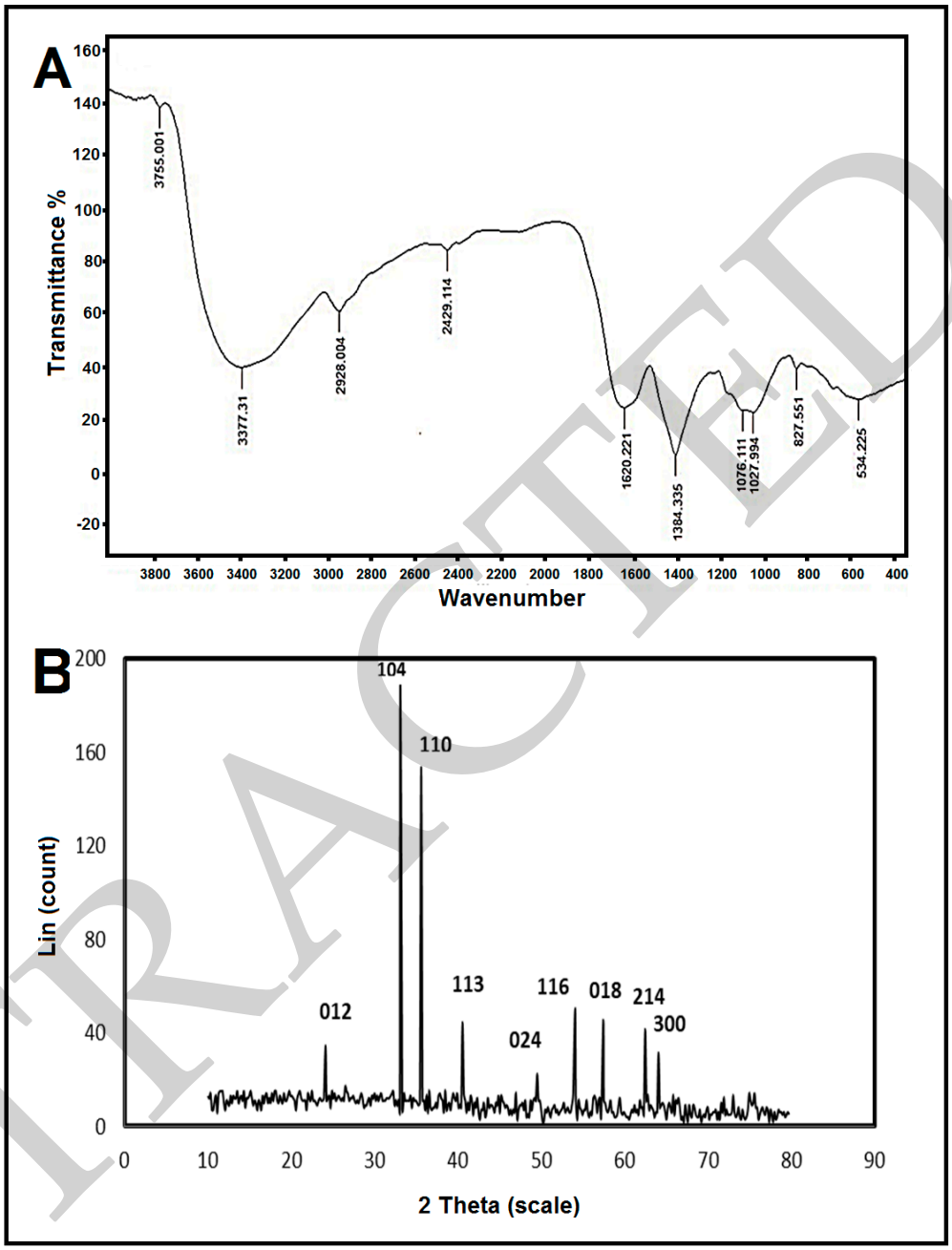


Figure 4. (**A**) FTIR spectrum and (**B**) XRD spectrum of Hem-NPs.

3.3.3. X-ray Diffraction (XRD)

To identify the phase of nanoparticles and their crystalline structures, X-ray diffraction was utilized. The XRD pattern is represented in Figure 4B. The reflection peaks in this pattern were in good agreement with Hem-NPs having the expected rhombohedral geometry (JCPDS-79-1741). Peaks of crystalline α-Fe_2O_3 NPs were found at 24.12°, 33.1°, 35.6°, 40.54°, 49.52°, 54.08°, 57.46°, 62.48°, and 64.08°. These peaks corresponded to the crystal planes of (012), (104), (110), (113), (024), (116), (122), (214), and (300), respectively [61]. According to Scherrer's formula (Equation (1)), for a peak at 35.6°, the crystallite size in the nanoscale range is 79.26 nm. This result is supported by that of Naz et al. [71], who discovered that Hem-NPs fabricated by Rhus punjabensis extract had diffraction signals of (012), (104), (110), (113), (024), (116), (018), (214), and (300), respectively. The outcome serves as evidence that proteins are crucial to the production of iron oxide nanoparticles and

RETRACTED

function as capping and stabilizing agents during the manufacture of hem-nanoparticles. These outcomes are consistent with prior studies that were utilized to create hem-NPs [72].

3.3.4. Transmission Electron Microscopy (TEM)

αFe_2O_3 NPs that were produced by biological synthesis had their morphology and size examined using TEM investigation [59]. TEM micrographs investigated that the particles were hexagonal in shape and monodispersely distributed without considerable integration (Figure 5A). Gaining control over the biogenic shape of bionanomaterials through green synthesis has the potential to open up a new, spectacular route for industrial-scale and eco-friendly applications [73]. The TEM image exhibits the well-dispersed green synthesized Hem-NPs without any aggregation, and the NPs size range was 75 to 80 nm. The results are consistent with [50], who used three fungal strains to successfully synthesis well-dispersed, spherical Fe_2O_3NPs with a size range of 18–32 nm. Bashir et al. [58] used Persea Americana seed extract for biosynthesis of spherical Hem-NPs with an average size of 70 nm. Recently, spherical MgO-NPs were effectively manufactured using Aspergillus carbonarious D-1 metabolites with sizes ranging from 20 to 80 nm [74].

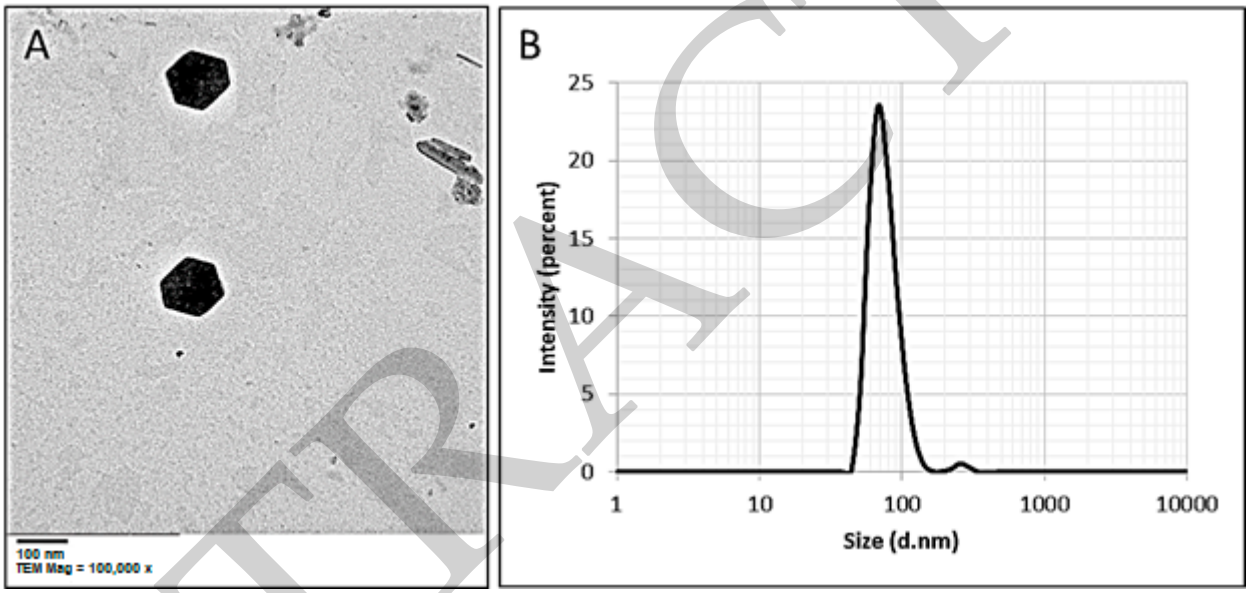


Figure 5. TEM image for Hem-NPs showing hexagonal shapes (**A**) and DLS analysis of the biosynthesized Hem-NPs (**B**).

3.3.5. Dynamic Light Scattering (DLS) Analysis

The DLS analysis based on hydrodynamic diameters was used to examine the size and distribution of biosynthesized Hem-NPs. According to the particle size distribution histogram, the volume intensity was 97.2% with an average hydrodynamic particle diameter of 78 nm (Figure 5B). Because of coating metabolites on the NPs surface, which are used for capping and stabilizing Hem-NPs, the average size produced by the DLS approach is larger than those obtained by TEM analysis. This revealed that the mean particles size of prepared Hem-NPs increases from 58 to 76 nm depending on the precursor concentration from 0.05 M to 0.45 M. According to Ahmed et al. [59], Hem-NPs were measured to have an average diameter of 26.53 nm by utilizing Punica granatum seed extract. By evaluating the polydispersity value, the DLS analysis offers additional details regarding the homogeneity of particles in the colloidal solution (PDI). As previously reported, the PDI value determined whether homogeneity was enhanced or lowered, with increased homogeneity occurring if the PDI value was less than 0.4 and decreased homogeneity occurring if the PDI value was greater than 0.4 [48]. The solution expands when the PDI value goes up

RETRACTED

over 1.0. The biosynthesized Hem-NPs colloidal solution in this study had a PDI value of 0.3, demonstrating that it was homogenous.

3.4. Antimicrobial Activity of Hem-NPs

Figure 6 and Table 1 show the results of an evaluation of the Hem-NPs' antimicrobial efficacy against Gram-positive, Gram-negative, unicellular, and multicellular fungi. The results showed that the Hem-NPs exhibited antibacterial activity against all tested bacterial strains, except *P. aeruginosa*, where the inhibition zones were 37.3 ± 1.52, 39.00 ± 1.00, and 46.33 ± 1.15 mm toward *E. coli*, *B. subtilis*, and *S. mutans*, respectively. However, none of the examined bacterial strains were inhibited by the biomass filtrate. Furthermore, the MIC was detected for these tested bacterial strains, where results showed that the MICs of Hem-NPs against *E. coli*, *B. subtilis*, and *S. mutans* were 125, 31.25, and 15.62 µg/mL respectively, as shown in Table 1. Tran et al. [75] reported that IO-NPs have a bactericidal effect against Staphylococcus aureus at 3000 µg/mL. According to Azam et al. [76], IO-NPs show antibacterial action against *B. subtilis* and *E. coli* where inhibition zones were 15 and 3 mm respectively. The antibacterial activity of IO-NPs is attributed to xidative stress generated by ROS [77]. ROS, including superoxide radicals (O_2^-), hydroxyl radicals (−OH), hydrogen peroxide (H_2O_2), and singlet oxygen ($^1O_2$), can cause damage to proteins and DNA in bacteria [78]. Also, bactericidal effects are attributed to the small size of nanoparticles, where Lee et al. [79] reported that IO-NPs have antibacterial activity against *E. coli*, this may be the result of tiny IO-NP particles (10–80 nm) penetrating the *E. coli* membrane during the attack on *E. coli*.

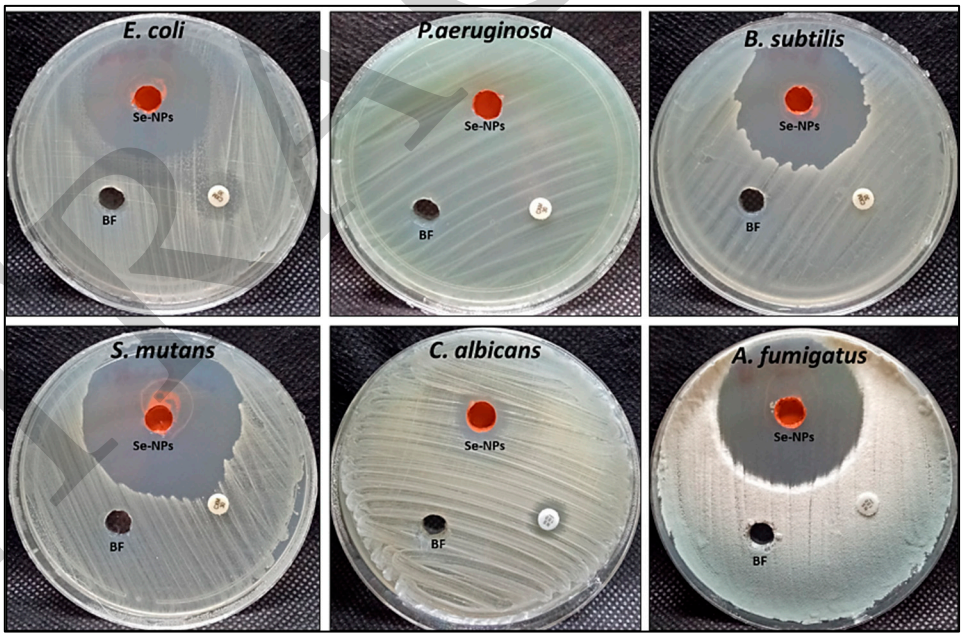


Figure 6. Antimicrobial activity of Hem-NPs using the agar well diffusion method.

Moreover, Hem-NPs showed antifungal activity against *C. albicans* and *A. fumigatus*, where inhibition zones were 14.13 ± 0.81 and 43.13 ± 1.03 mm respectively, as shown in Table 1. Biomass filtrate did not give antifungal activity, but nystatin gave little inhibition on *C. albicans* only. Then, different concentrations of Hem-NPs (3.9–4000 µg/mL) were tested against *C. albicans* and *A. fumigatus*, results revealed that IO-NPs had weak antifungal activity against *C. albicans* where the MIC was 2000 µg/mL. On the other hand, Hem-NPs exhibited promising antifungal activity against *A. fumigatus* at concentrations from 4000 to 62.5 µg/mL, while concentrations lower than 62.5 µg/mL did not give any activity; this indicates the MIC was 62.5 µg/mL. According to Devi et al. [61], green synthesized IO-NPs showed potential antifungal action against *A. niger* and Mucor piriformis. Antifungal

RETRACTED

activity of IO-NPs is attributed to the direct interaction between NPs and cell surfaces, leading to the induction oxidative stress in fungus cells, and affects the permeability of membranes, which leads to cell growth and cell death [80].

Table 1. Effect of different concentrations of Hem-NPs on bacterial and fungal strains.

Compounds		Inhibition Zone/mm					
		E. coli	*P. aeruginosa*	*B. subtilis*	*S. mutans*	*C. albicans*	*A. fumigatus*
Hem-NPs (µg/mL)	4000	37.3 ± 1.52 [a]	0 ± 0.00	39.00 ± 1.00 [a]	46.33 ± 1.15 [a]	14.13 ± 0.81 [a]	43.13 ± 1.03 [a]
	2000	31 ± 1.00 [b]	0 ± 0.00	34.67 ± 0.58 [b]	40.93 ± 0.9 [b]	8.67 ± 0.58 [b]	35.23 ± 0.68 [b]
	1000	24.3 ± 1.15 [c]	0 ± 0.00	30.83 ± 0.76 [c]	35.63 ± 0.55 [c]	0 ±0. 00 [c]	28.33 ± 0.58 [c]
	500	18.5 ± 0.5 [d]	0 ± 0.00	25.40 ± 0.53 [d]	29.33 ± 0.58 [d]	0 ± 0.00 [c]	24.07 ± 0.90 [d]
	250	12.8 ± 0.76 [e]	0 ± 0.00	20.17 ± 0.76 [e]	22.00 ± 1.00 [e]	0 ± 0.00 [c]	18.30 ± 0.52 [e]
	125	8.3 ± 0.57 [f]	0 ± 0.00	16.00 ± 1.00 [f]	17.83 ± 0.29 [f]	0 ± 0.00 [c]	13.90 ± 0.66 [f]
	62.5	0 ± 0.00 [g]	0 ± 0.00	10.57 ± 0.81 [g]	13.30 ± 0.75 [g]	0 ± 0.00 [c]	9.00 ± 1.00 [g]
	31.25	0 ± 0.00 [g]	0 ± 0.00	8.33 ± 0.58 [h]	10.33 ± 0.58 [h]	0 ± 0.00 [c]	0 ± 0.00 [h]
	15.62	0 ± 0.00 [g]	0 ± 0.00	0 ± 0.00 [i]	8.23 ± 0.40 [i]	0 ± 0.00 [c]	0 ± 0.00 [h]
	7.81	0 ± 0.00 [g]	0 ± 0.00	0 ± 0.00 [i]	0 ± 0.00 [j]	0 ± 0.00 [c]	0 ± 0.00 [h]
	3.9	0 ±0.00 [g]	0 ± 0.00	0 ± 0.00 [i]	0 ± 0.00 [j]	0 ± 0.00 [c]	0 ± 0.00 [h]
BF *		0 ± 0.00	0 ±0.00	0 ± 0.00	0 ± 0.00	0 ± 0.00	0 ± 0.00
CXM/NS **		12.2 ± 0.44	0 ± 0.00	0 ± 0.00	0 ± 0.00	11.7 ± 0.35	0 ± 0.00

* BF means biomass filtrate, ** CXM/NS means Cefuroxime/Nystatin. Superscript letters from a to h reveal the power of significance.

3.5. Photocatalytic Degradation of Crystal Violet Dye Using Hem-NPs

A light source is used to irradiate nanoparticles, and the degradation process either involves directly applying high-energy light sources to the surface of the nanomaterials or utilizing a photosensitization method. In the case of direct photocatalytic degradation, photoexcitation occurs when electrons are moved from the valence band (filled) to the conduction band using energy from light [81]. In this research, in order to conduct a comparative analysis, the potential of Hem-NPs for the decolorization of crystal violet dye was examined at various Hem-NP concentrations (0.25, 0.5, 0.75, and 1.0 mg mL^{-1}) and contact times (30.0, 60.0, 90.0, 120.0, 150.0, 180.0, and 210.0 min) under both light and dark conditions. The data analysis demonstrated that the catalytic activity of Hem-NPs was dose and time-dependent. Interestingly, exposure to sunlight increased Hem-NPs' biodegradation more than exposure to dark conditions (Figure 7A–D). At 0.25 mg mL^{-1} Hem-NPs, the decolourization percentages reached up to 22 % ± 0.03% and 10% ± 0.02% under sunlight and dark conditions, respectively, after 210 min as compared with the control (4% ± 0.001% after 210 min). At 0.5 mg mL^{-1} of Hem-NPs, the decolourization percentages under sunlight stimulation began at 10% ± 0.03 after 30 min and increased to 57.4% ± 0.04 after 180 min. Furthermore, at 0.75 mg mL^{-1} of Hem-NPs, the decolourization percentages under sunlight and dark conditions were 81.3% ± 0.04% and 47.7% ± 0.04% after 150 min, respectively. The highest decolourization was achieved at 1.0 mg mL^{-1} of Hem-NPs concentration in the presence of sunlight with percentages of 97.5% ± 0.055% after 150 min, whereas in the dark ambience, at the same NPs concentrations, the decolourization was 66.3% ± 0.036% after 210 min. According to these results, the best condition was 1.0 mg mL^{-1} of Hem-NPs after 150 min of contact time. In order for biosynthesized MgO-NPs to be effective in degrading textile wastewater, Fouda et al. [82] observed that light stimulators must be present. Saad et al. [83] reported that, the removal of CV dye was found to be 94.29% by using polyaniline nanoparticles (PANP). According to Rufus et al. [84], the addition of hematite nanoparticles as a catalyst caused the intensity of absorption to gradually decrease and the colour of

RETRACTED

the dye to continue fading, implying a significant reduction in MB. For samples P, Q, and R, respectively, the reactions were completed in 40, 34, and 30 min. The breakdown of the non-biodegradable dye RhB in the presence of H_2O_2 was proven by Popov et al. [85] who reported that, the creation of hematite nanoparticles and their use as photocatalysts (heterogeneous photo-Fenton process). The highest dye decolourization is caused by an increase in Hem-NPs concentration because there are more adsorption sites on the NPs surface [86]. The time required for decolourization and degradation of either pure or one dye was compared to complex solutions that comprise several types of dye or unknown chemicals [87].

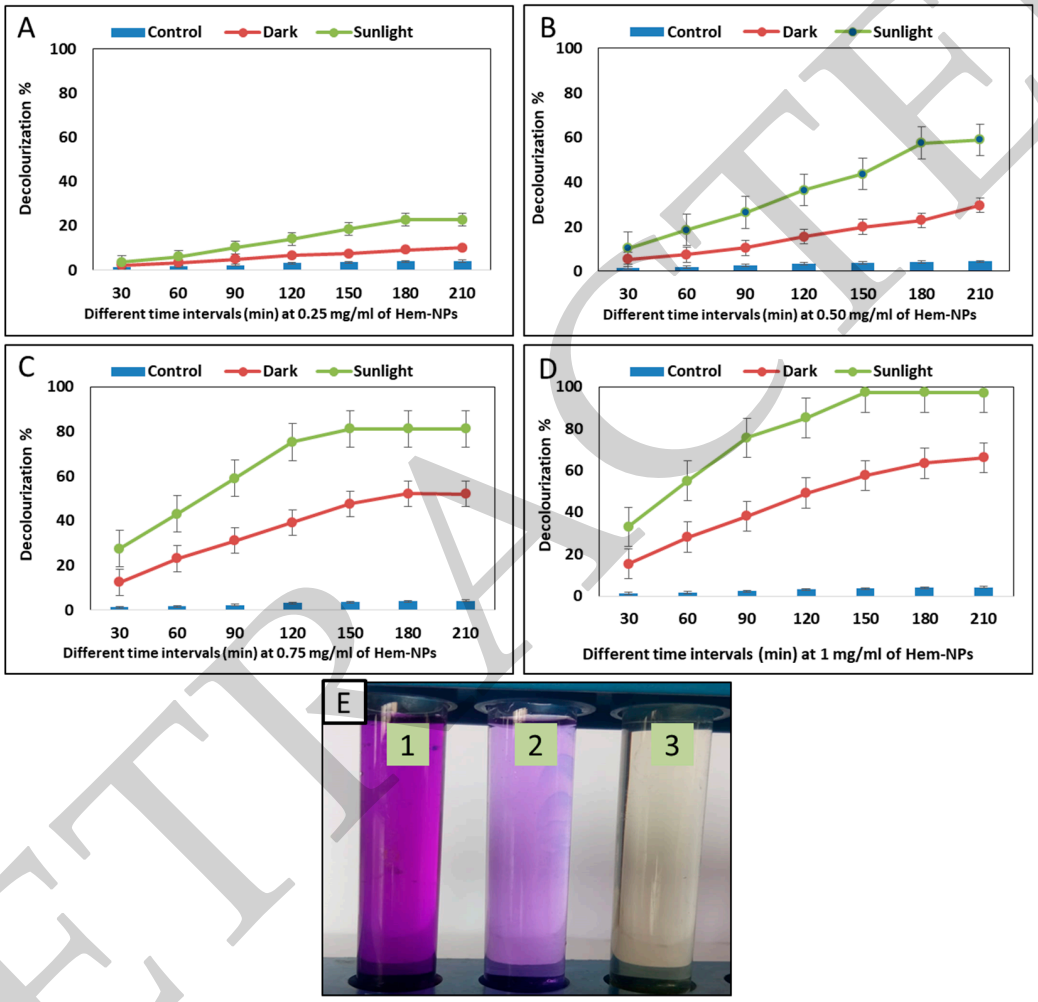


Figure 7. Decolorization percentages of crystal violet dye at different Hem-NPs concentrations, in different stimulation conditions (sunlight and dark), and for different contact times (**A**–**D**). Dye decolorization under sunlight and dark conditions (**E 1**–**3**), where **E1** was the dye control, **E2** was the dye under the dark condition, and **E3** was the dye under the sunlight condition.

The effectiveness of band gap energy α-Fe_2O_3 NPs in dye decolorization may be attributed to the production of reactive hydroxyl radicals, which promote decolorization [88]. In the electronic structure of α-Fe_2O_3, the conductance band (CB) and valence band (VB) were the two band levels that could be seen. The sunshine photoexcites electrons in the valence band of Fe_2O_3 into their conduction band. The separation of charges caused by the electrons in the conduction band led to the creation of $O_2^{\bullet -}$ radicals from O_2, which are then changed into hydroxyl radicals. Additionally, the produced hole (h^+) tends to break down H_2O into the hydrogen (H^+) ion and the hydroxyl radical ($OH^{\bullet}$). Finally, the

RETRACTED

hydroxyl radical ($OH^{\bullet}$) formed is highly reactive and acts as a powerful oxidizing agent, which may be utilized for the degradation of dyes and other pollutants [89–91].

$$e^{-} + O_2 \rightarrow O_2^{-} \quad (2)$$

$$h^{+} + H_2O \rightarrow {}^{\bullet}OH + H^{+} \quad (3)$$

$$\text{Dyes} + {}^{\bullet}OH \rightarrow CO_2 + H_2O + \text{non-biodegradable compounds} \quad (4)$$

El-Naggar, Shoueir [92] discovered that by absorbing light and creating holes, the metal oxides of NPs have the ability to produce charge separation, which reduces or oxidizes organic compounds, including organic colors. When compared with dark settings, the photocatalytic activities in this study were caused by the activation of biosynthesized Hem-NPs via sunshine stimulators (Figure 7E).

3.6. Recyclability of Hem-NPs

The reusability and photostability of the catalysts are key dynamics to evaluating their catalytic efficacy in order to make the process cost-effective [59]. The stability of biosynthesized Hem-NPs as a biocatalyst for reuse in dye wastewater treatment was examined in this work. The stability test was carried out under ideal conditions (1.0 mg mL^{-1} biocatalyst, 150 min contact time under photocatalytic sunlight) as shown in Figure 8. Every cycle was finished with a centrifugation step to remove the catalyst, followed by three washes with deionized water and an hour of drying at 100 °C to remove any residual water. The dried catalyst was then utilized as a bio-inoculant for the subsequent cycle. The decolourization percentages of crystal violet dye were reduced to up to 63.5% ± 1.04% when it was repeated for the fourth cycle, according to data observed in Figure 7A,B. According to Li et al. [93], in the first cycle, reactive blue 19, brilliant green, crystal violet, azophloxine dye and malachite green degraded at rates of 99, 93, 79, 88, and 81 percent, respectively. After ten reuses, the dye removal efficiencies of the five dyes were found to be 94, 80, 71, 78, and 65 percent, respectively. These results are in line with earlier research [94,95]. The unavoidable decrease in catalyst performance was caused by the catalytic site degradation, metal leaching concentration, and adsorption of intermediate products on catalytic sites [59].

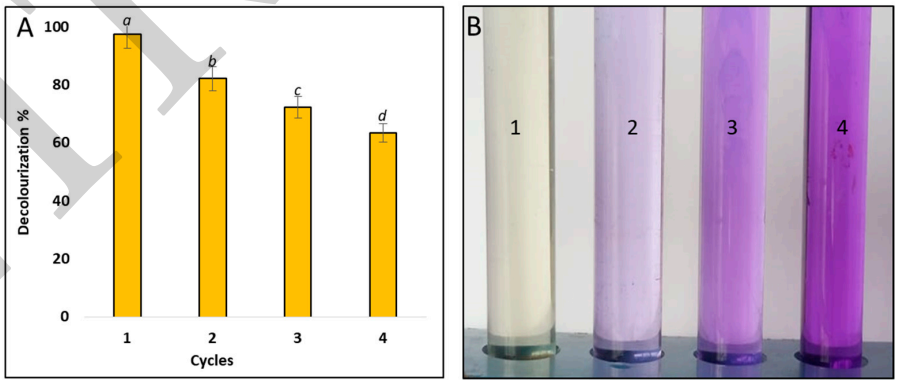


Figure 8. Hem-NP recycling in the crystal violet dye removal process (**A**) and crystal violet dye removal cycle color changes (**B**) at 4 cycles (1–4). Superscript letters from a to d reveal the power of significance.

4. Conclusions

In the current work, an *A. niger* AH1 biomass filtrate was used to effectively biosynthesize Hem-NPs. UV- Visible spectroscopy, FTIR spectroscopy, XRD, TEM, and DLS analyses were used to characterize the biosynthesized Hem-NPs. The average particle size was determined to be 78.5 nm. The UV- Visible absorbance spectral analysis revealed a distinct peak at a wavelength of 490 nm, while the DLS analysis revealed their size distribution. The NPs' existence and crystallinity were confirmed via the XRD examination. TEM confirmed

RETRACTED

the Hem-NPs' hexagonal form and a size range of 75 to 80 nm. The generation of Hem-NPs was influenced by the reaction time, pH, and precursor concentration. To produce a high yield of α-Fe_2O_3 NPs, 3 mM of the precursor, 36 h, and a pH of 9 were needed. Hem-NPs showed effective antibacterial activity against Gram-positive and Gram-negative bacteria, as well as antifungal efficiency against single-celled and multicellular fungi. Furthermore, Hem-NPs demonstrated 97 percent photocatalytic destruction of CV dye in 150 min. The findings demonstrated that Hem-NPs have a high potential for dye degradation; thus, these Hem-NPs may be used in the future to degrade dangerous colors from contaminated water.

Author Contributions: Conceptualization, E.S. and A.H.H.; methodology, E.S., A.H.H., F.M.E. and S.S.S. software, E.S. and A.H.H.; validation, E.S. and A.H.H.; formal analysis, E.S. and A.H.H.; investigation, E.S., A.H.H., F.M.E., A.A.A.-A., A.A.A. and S.S.S. resources, E.S., A.H.H., F.M.E., A.A.A.-A., A.A.A. and S.S.S., data curation, E.S. and A.H.H.; writing—original draft preparation, E.S., A.H.H., F.M.E., A.A.A.-A., A.A.A. and S.S.S., writing—review and editing, E.S., A.H.H., F.M.E., A.A.A.-A., A.A.A. and S.S.S., project administration, A.A.A.-A.; funding acquisition, A.A.A.-A. All authors have read and agreed to the published version of the manuscript.

Funding: The authors extend their appreciation to the Researcher Supporting Project (number RSP2022R505), King Saud University, Riyadh, Saudi Arabia, for funding this work.

Institutional Review Board Statement: Not Applicable.

Informed Consent Statement: Not Applicable.

Data Availability Statement: All data generated or analyzed during this study are included in this published article.

Acknowledgments: The authors express their sincere thanks to the Faculty of Science (Boys), Al-Azhar University, Cairo, Egypt, for providing the necessary research facilities.

Conflicts of Interest: The authors declare no conflict of interest.

References

1. Vishani, D.B.; Shrivastav, A. Enzymatic decolorization and degradation of azo dyes. In *Development in Wastewater Treatment Research and Processes*; Elsevier: Amsterdam, The Netherlands, 2022; pp. 419–432.
2. Sridevi, M.; Nirmala, C.; Jawahar, N.; Arthi, G.; Vallinayagam, S.; Sharma, V.K. Role of nanomaterial's as adsorbent for heterogeneous reaction in waste water treatment. *J. Mol. Struct.* **2021**, *1241*, 130596. [CrossRef]
3. Kishor, R.; Purchase, D.; Saratale, G.D.; Saratale, R.G.; Ferreira, L.F.R.; Bilal, M.; Chandra, R.; Bharagava, R.N. Ecotoxicological and health concerns of persistent coloring pollutants of textile industry wastewater and treatment approaches for environmental safety. *J. Environ. Chem. Eng.* **2021**, *9*, 105012. [CrossRef]
4. Elgarahy, A.; Elwakeel, K.; Mohammad, S.; Elshoubaky, G. A critical review of biosorption of dyes, heavy metals and metalloids from wastewater as an efficient and green process. *Clean. Eng. Technol.* **2021**, *4*, 100209. [CrossRef]
5. Ahmed, N.E.; Salem, S.S.; Hashem, A.H. Statistical optimization, partial purification, and characterization of phytase produced from talaromyces purpureogenus nsa20 using potato peel waste and its application in dyes de-colorization. *Biointerface Res. Appl. Chem.* **2022**, *12*, 4417–4431. [CrossRef]
6. El-Aswar, E.I.; Ramadan, H.; Elkik, H.; Taha, A.G. A comprehensive review on preparation, functionalization and recent applications of nanofiber membranes in wastewater treatment. *J. Environ. Manag.* **2022**, *301*, 113908. [CrossRef] [PubMed]
7. Crini, G.; Lichtfouse, E.; Wilson, L.D.; Morin-Crini, N. Conventional and non-conventional adsorbents for wastewater treatment. *Environ. Chem. Lett.* **2019**, *17*, 195–213. [CrossRef]
8. Selim, M.T.; Salem, S.S.; Mohamed, A.A.; El-Gamal, M.S.; Awad, M.F.; Fouda, A. Biological treatment of real textile effluent using aspergillus flavus and fusarium oxysporium and their consortium along with the evaluation of their phytotoxicity. *J. Fungi* **2021**, *7*, 193. [CrossRef]
9. Salem, S.S.; Hammad, E.N.; Mohamed, A.A.; El-Dougdoug, W. A Comprehensive Review of Nanomaterials: Types, Synthesis, Characterization, and Applications. *Biointerface Res. Appl. Chem.* **2022**, *13*, 41. [CrossRef]
10. Salem, S.S.; Fouda, A. Green Synthesis of Metallic Nanoparticles and Their Prospective Biotechnological Applications: An Overview. *Biol. Trace Elem. Res.* **2021**, *199*, 344–370. [CrossRef]
11. Patel, P.; Nandi, A.; Jha, E.; Sinha, A.; Mohanty, S.; Panda, P.K.; Mishra, S.; Verma, S.K.; Suar, M. Magnetic nanoparticles: Fabrication, characterization, properties, and application for environment sustainability. In *Magnetic Nanoparticle-Based Hybrid Materials*; Elsevier: Amsterdam, The Netherlands, 2021; pp. 33–64.
12. Salem, S.S. Bio-fabrication of Selenium Nanoparticles Using Baker's Yeast Extract and Its Antimicrobial Efficacy on Food Borne Pathogens. *Appl. Biochem. Biotechnol.* **2022**, *194*, 1898–1910. [CrossRef]

RETRACTED

13. Abd Elkodous, M.; El-Husseiny, H.M.; El-Sayyad, G.S.; Hashem, A.H.; Doghish, A.S.; Elfadil, D.; Radwan, Y.; El-Zeiny, H.M.; Bedair, H.; Ikhdair, O.A. Recent advances in waste-recycled nanomaterials for biomedical applications: Waste-to-wealth. *Nanotechnol. Rev.* **2021**, *10*, 1662–1739. [CrossRef]
14. Elbahnasawy, M.A.; Shehabeldine, A.M.; Khattab, A.M.; Amin, B.H.; Hashem, A.H. Green biosynthesis of silver nanoparticles using novel endophytic Rothia endophytica: Characterization and anticandidal activity. *J. Drug Deliv. Sci. Technol.* **2021**, *62*, 102401. [CrossRef]
15. Elbasuney, S.; El-Sayyad, G.S.; Tantawy, H.; Hashem, A.H. Promising antimicrobial and antibiofilm activities of reduced graphene oxide-metal oxide (RGO-NiO, RGO-AgO, and RGO-ZnO) nanocomposites. *RSC Adv.* **2021**, *11*, 25961–25975. [CrossRef] [PubMed]
16. Hasanin, M.; Al Abboud, M.A.; Alawlaqi, M.M.; Abdelghany, T.M.; Hashem, A.H. Ecofriendly Synthesis of Biosynthesized Copper Nanoparticles with Starch-Based Nanocomposite: Antimicrobial, Antioxidant, and Anticancer Activities. *Biol. Trace Elem. Res.* **2021**, *200*, 2099–2112. [CrossRef]
17. Hasanin, M.; Elbahnasawy, M.A.; Shehabeldine, A.M.; Hashem, A.H. Ecofriendly preparation of silver nanoparticles-based nanocomposite stabilized by polysaccharides with antibacterial, antifungal and antiviral activities. *BioMetals* **2021**, *34*, 1313–1328. [CrossRef]
18. Hashem, A.H.; Al Abboud, M.A.; Alawlaqi, M.M.; Abdelghany, T.M.; Hasanin, M. Synthesis of Nanocapsules Based on Biosynthesized Nickel Nanoparticles and Potato Starch: Antimicrobial, Antioxidant, and Anticancer Activity. *Starke* **2022**, *74*, e2100165. [CrossRef]
19. Hashem, A.H.; Salem, S.S. Green and ecofriendly biosynthesis of selenium nanoparticles using Urtica dioica (stinging nettle) leaf extract: Antimicrobial and anticancer activity. *Biotechnol. J.* **2021**, *17*, 2100432. [CrossRef]
20. Al-Rajhi, A.M.H.; Salem, S.S.; Alharbi, A.A.; Abdelghany, T.M. Ecofriendly synthesis of silver nanoparticles using Kei-apple (Dovyalis caffra) fruit and their efficacy against cancer cells and clinical pathogenic microorganisms. *Arab. J. Chem.* **2022**, *15*, 103927. [CrossRef]
21. Mazari, S.A.; Ali, E.; Abro, R.; Khan, F.S.A.; Ahmed, I.; Ahmed, M.; Nizamuddin, S.; Siddiqui, T.H.; Hossain, N.; Mubarak, N.M. Nanomaterials: Applications, waste-handling, environmental toxicities, and future challenges–A review. *J. Environ. Chem. Eng.* **2021**, *9*, 105028. [CrossRef]
22. Hammad, E.N.; Salem, S.S.; Mohamed, A.A.; El-Dougdoug, W. Environmental Impacts of Ecofriendly Iron Oxide Nanoparticles on Dyes Removal and Antibacterial Activity. *Appl. Biochem. Biotechnol.* **2022**. [CrossRef]
23. Leonel, A.G.; Mansur, A.A.; Mansur, H.S. Advanced functional nanostructures based on magnetic iron oxide nanomaterials for water remediation: A review. *Water Res.* **2021**, *190*, 116693. [CrossRef] [PubMed]
24. Annu, A.A.; Ahmed, S. Green synthesis of metal, metal oxide nanoparticles, and their various applications. *Handb. Ecomater.* **2018**, *2018*, 1–45.
25. LaGrow, A.P.; Besenhard, M.O.; Hodzic, A.; Sergides, A.; Bogart, L.K.; Gavriilidis, A.; Thanh, N.T.K. Unravelling the growth mechanism of the co-precipitation of iron oxide nanoparticles with the aid of synchrotron X-ray diffraction in solution. *Nanoscale* **2019**, *11*, 6620–6628. [CrossRef] [PubMed]
26. Parashar, M.; Shukla, V.K.; Singh, R. Metal oxides nanoparticles via sol–gel method: A review on synthesis, characterization and applications. *J. Mater. Sci. Mater. Electron.* **2020**, *31*, 3729–3749. [CrossRef]
27. Aghazadeh, M.; Ganjali, M.R. Evaluation of supercapacitive and magnetic properties of Fe_3O_4 nano-particles electrochemically doped with dysprosium cations: Development of a novel iron-based electrode. *Ceram. Int.* **2018**, *44*, 520–529. [CrossRef]
28. Young, C.; Wang, J.; Kim, J.; Sugahara, Y.; Henzie, J.; Yamauchi, Y. Controlled chemical vapor deposition for synthesis of nanowire arrays of metal–organic frameworks and their thermal conversion to carbon/metal oxide hybrid materials. *Chem. Mater.* **2018**, *30*, 3379–3386. [CrossRef]
29. Zhong, G.; Xu, S.; Chen, C.; Kline, D.J.; Giroux, M.; Pei, Y.; Jiao, M.; Liu, D.; Mi, R.; Xie, H. Synthesis of metal oxide nanoparticles by rapid, high-temperature 3D microwave heating. *Adv. Funct. Mater.* **2019**, *29*, 1904282. [CrossRef]
30. Khashan, K.S.; Sulaiman, G.M.; Mahdi, R. The effect of laser energy on the properties of carbon nanotube—iron oxide nanoparticles composite prepared via pulsed laser ablation in liquid. *Mater. Res. Express* **2018**, *5*, 105004. [CrossRef]
31. Ribeiro, A.I.; Dias, A.M.; Zille, A. Synergistic Effects Between Metal Nanoparticles and Commercial Antimicrobial Agents: A Review. *ACS Appl. Nano Mater.* **2022**, *5*, 3030–3064. [CrossRef]
32. Ahmed, S.F.; Mofijur, M.; Rafa, N.; Chowdhury, A.T.; Chowdhury, S.; Nahrin, M.; Islam, A.S.; Ong, H.C. Green approaches in synthesising nanomaterials for environmental nanobioremediation: Technological advancements, applications, benefits and challenges. *Environ. Res.* **2022**, *204*, 111967. [CrossRef]
33. Nagajyothi, P.C.; Prabhakar Vattikuti, S.V.; Devarayapalli, K.C.; Yoo, K.; Shim, J.; Sreekanth, T.V.M. Green synthesis: Photocatalytic degradation of textile dyes using metal and metal oxide nanoparticles-latest trends and advancements. *Crit. Rev. Environ. Sci. Technol.* **2020**, *50*, 2617–2723. [CrossRef]
34. Goutam, S.P.; Saxena, G.; Roy, D.; Yadav, A.K.; Bharagava, R.N. Green synthesis of nanoparticles and their applications in water and wastewater treatment. In *Bioremediation of Industrial Waste for Environmental Safety*; Springer: Berlin/Heidelberg, Germany, 2020; pp. 349–379.
35. Fouad, D.E.; Zhang, C.; El-Didamony, H.; Yingnan, L.; Mekuria, T.D.; Shah, A.H. Improved size, morphology and crystallinity of hematite (α-Fe_2O_3) nanoparticles synthesized via the precipitation route using ferric sulfate precursor. *Results Phys.* **2019**, *12*, 1253–1261. [CrossRef]

REJECTED

36. Hasanin, M.; Hashem, A.H.; Lashin, I.; Hassan, S.A. In vitro improvement and rooting of banana plantlets using antifungal nanocomposite based on myco-synthesized copper oxide nanoparticles and starch. *Biomass Convers. Biorefinery* **2021**, 1–11. [CrossRef]
37. Zakariya, N.A.; Majeed, S.; Jusof, W.H.W. Investigation of antioxidant and antibacterial activity of iron oxide nanoparticles (IONPS) synthesized from the aqueous extract of *Penicillium* spp. *Sens. Int.* **2022**, *3*, 100164. [CrossRef]
38. Dash, P.; Raut, S.; Jena, M.; Nayak, B. Harnessing the biomedical properties of ferromagnetic α-Fe_2O_3 NPs with a plausible formation mechanism. *Ceram. Int.* **2020**, *46*, 26190–26204. [CrossRef]
39. Fouda, A.; Hassan, S.E.-D.; Abdel-Rahman, M.A.; Farag, M.M.; Shehal-deen, A.; Mohamed, A.A.; Alsharif, S.M.; Saied, E.; Moghanim, S.A.; Azab, M.S. Catalytic degradation of wastewater from the textile and tannery industries by green synthesized hematite (α-Fe_2O_3) and magnesium oxide (MgO) nanoparticles. *Curr. Res. Biotechnol.* **2021**, *3*, 29–41. [CrossRef]
40. Hassan, S.E.-D.; Fouda, A.; Saied, E.; Farag, M.; Eid, A.M.; Barghoth, M.G.; Awad, M.A.; Hamza, M.F.; Awad, M.F. Rhizopus Oryzae-mediated green synthesis of magnesium oxide nanoparticles (MgO-NPs): A promising tool for antimicrobial, mosquitocidal action, and tanning effluent treatment. *J. Fungi* **2021**, *7*, 372. [CrossRef]
41. Fouda, A.; Hassan, S.E.-D.; Saied, E.; Azab, M.S. An eco-friendly approach to textile and tannery wastewater treatment using maghemite nanoparticles (γ-Fe_2O_3-NPs) fabricated by Penicillium expansum strain (Kw). *J. Environ. Chem. Eng.* **2021**, *9*, 104693. [CrossRef]
42. Fouda, A.; Eid, A.M.; Abdel-Rahman, M.A.; El-Belely, E.F.; Awad, M.A.; Hassan, S.E.-D.; Al-Faifi, Z.E.; Hamza, M.F. Enhanced Antimicrobial, Cytotoxicity, Larvicidal, and Repellence Activities of Brown Algae, Cystoseira crinita-Mediated Green Synthesis of Magnesium Oxide Nanoparticles. *Front. Bioeng. Biotechnol.* **2022**, *10*, 849921. [CrossRef]
43. Standards, N.C.F.C.L. *Reference Method for Broth Dilution Antifungal Susceptibility Testing of Yeasts*; National Committee for Clinical Laboratory Standards: Wayne, PA, USA, 2002.
44. Valgas, C.; Souza, S.M.D.; Smânia, E.; Smânia, A. Screening methods to determine antibacterial activity of natural products. *Braz. J. Microbiol.* **2007**, *38*, 369–380. [CrossRef]
45. Dacrory, S.; Hashem, A.H.; Hasanin, M. Synthesis of cellulose based amino acid functionalized nano-biocomplex: Characterization, antifungal activity, molecular docking and hemocompatibility. *Environ. Nanotechnol. Monit. Manag.* **2021**, *15*, 100453. [CrossRef]
46. Oladipo, A.A.; Ifebajo, A.O.; Gazi, M. Magnetic LDH-based CoO–$NiFe_2O_4$ catalyst with enhanced performance and recyclability for efficient decolorization of azo dye via Fenton-like reactions. *Appl. Catal. B Environ.* **2019**, *243*, 243–252. [CrossRef]
47. Chatterjee, S.; Mahanty, S.; Das, P.; Chaudhuri, P.; Das, S. Biofabrication of iron oxide nanoparticles using manglicolous fungus Aspergillus niger BSC-1 and removal of Cr (VI) from aqueous solution. *Chem. Eng. J.* **2020**, *385*, 123790. [CrossRef]
48. Srivastava, N.; Srivastava, M.; Alhazmi, A.; Mohammad, A.; Khan, S.; Pal, D.B.; Haque, S.; Singh, R.; Mishra, P.; Gupta, V.K. Sustainable green approach to synthesize Fe_3O_4/α-Fe_2O_3 nanocomposite using waste pulp of Syzygium cumini and its application in functional stability of microbial cellulases. *Sci. Rep.* **2021**, *11*, 24371. [CrossRef] [PubMed]
49. Fouda, A.; Awad, M.A.; Eid, A.M.; Saied, E.; Barghoth, M.G.; Hamza, M.F.; Awad, M.F.; Abdelbary, S.; Hassan, S.E.-D. An Eco-Friendly Approach to the Control of Pathogenic Microbes and Anopheles stephensi Malarial Vector Using Magnesium Oxide Nanoparticles (Mg-NPs) Fabricated by Penicillium chrysogenum. *Int. J. Mol. Sci.* **2021**, *22*, 5096. [CrossRef] [PubMed]
50. Mohamed, A.A.; Abu-Elghait, M.; Ahmed, N.E.; Salem, S.S. Eco-friendly mycogenic synthesis of ZnO and CuO nanoparticles for in vitro antibacterial, antibiofilm, and antifungal applications. *Biol. Trace Elem. Res.* **2021**, *199*, 2788–2799. [CrossRef]
51. Mahanty, S.; Bakshi, M.; Ghosh, S.; Chatterjee, S.; Bhattacharyya, S.; Das, P.; Das, S.; Chaudhuri, P. Green synthesis of iron oxide nanoparticles mediated by filamentous fungi isolated from Sundarban mangrove ecosystem, India. *BioNanoScience* **2019**, *9*, 637–651. [CrossRef]
52. Pallela, P.N.V.K.; Ummey, S.; Ruddaraju, L.K.; Gadi, S.; Cherukuri, C.S.; Barla, S.; Pammi, S.V.N. Antibacterial efficacy of green synthesized α-Fe_2O_3 nanoparticles using Sida cordifolia plant extract. *Heliyon* **2019**, *5*, e02765. [CrossRef] [PubMed]
53. Alagiri, M.; Hamid, S.B.A. Green synthesis of α-Fe_2O_3 nanoparticles for photocatalytic application. *J. Mater. Sci. Mater. Electron.* **2014**, *25*, 3572–3577. [CrossRef]
54. Karade, V.C.; Parit, S.B.; Dawkar, V.V.; Devan, R.S.; Choudhary, R.J.; Kedge, V.V.; Pawar, N.V.; Kim, J.H.; Chougale, A.D. A green approach for the synthesis of α-Fe2O3 nanoparticles from Gardenia resinifera plant and it's In vitro hyperthermia application. *Heliyon* **2019**, *5*, e02044. [CrossRef] [PubMed]
55. Vinayagam, R.; Pai, S.; Varadavenkatesan, T.; Narasimhan, M.K.; Narayanasamy, S.; Selvaraj, R. Structural characterization of green synthesized α-Fe_2O_3 nanoparticles using the leaf extract of Spondias dulcis. *Surf. Interfaces* **2020**, *20*, 100618. [CrossRef]
56. Abbas, H.S.; Akilandeswari, K.; Muddukrishnaiah, K. The antifungal and antiovarian cancer properties of α-Fe_2O_3 and α-Fe_2O_3/Zno nanostructures synthesized by Spirulina platensis. *IET Nanobiotechnol.* **2020**, *14*, 774–784. [CrossRef] [PubMed]
57. Yoonus, J.; Resmi, R.; Beena, B. Evaluation of antibacterial and anticancer activity of green synthesized iron oxide (α-Fe_2O_3) nanoparticles. *Mater. Today Proc.* **2021**, *46*, 2969–2974. [CrossRef]
58. Bashir, A.K.H.; Furqan, C.M.; Bharuth-Ram, K.; Kaviyarasu, K.; Tchokonté, M.B.T.; Maaza, M. Structural, optical and Mössbauer investigation on the biosynthesized α-Fe_2O_3: Study on different precursors. *Phys. E Low-Dimens. Syst. Nanostruct.* **2019**, *111*, 152–157. [CrossRef]
59. Ahmed, A.; Usman, M.; Yu, B.; Shen, Y.; Cong, H. Sustainable fabrication of hematite (α-Fe_2O_3) nanoparticles using biomolecules of Punica granatum seed extract for unconventional solar-light-driven photocatalytic remediation of organic dyes. *J. Mol. Liq.* **2021**, *339*, 116729. [CrossRef]
60. Asoufi, H.M.; Al-Antary, T.M.; Awwad, A.M. Green route for synthesis hematite (α-Fe_2O_3) nanoparticles: Toxicity effect on the green peach aphid, Myzus persicae (Sulzer). *Environ. Nanotechnol. Monit. Manag.* **2018**, *9*, 107–111. [CrossRef]

RETRACTED

61. Devi, H.S.; Boda, M.A.; Shah, M.A.; Parveen, S.; Wani, A.H. Green synthesis of iron oxide nanoparticles using Platanus orientalis leaf extract for antifungal activity. *Green Process. Synth.* **2019**, *8*, 38–45. [CrossRef]
62. Taghavi Fardood, S.; Ramazani, A.; Golfar, Z.; Woo Joo, S. Green Synthesis of α-Fe_2O (hematite) Nanoparticles using Tragacanth Gel. *J. Appl. Chem. Res.* **2017**, *11*, 19–27.
63. Maksoud, M.A.; Fahim, R.A.; Bedir, A.G.; Osman, A.I.; Abouelela, M.M.; El-Sayyad, G.S.; Abd Elkodous, M.; Mahmoud, A.S.; Rabee, M.M.; Ala'a, H. Engineered magnetic oxides nanoparticles as efficient sorbents for wastewater remediation: A review. *Environ. Chem. Lett.* **2021**, *20*, 519–562. [CrossRef]
64. Sarkar, J.; Mollick, M.; Rahaman, M.; Chattopadhyay, D.; Acharya, K. An eco-friendly route of γ-Fe_2O_3 nanoparticles formation and investigation of the mechanical properties of the HPMC-γ-Fe_2O_3 nanocomposites. *Bioprocess Biosyst. Eng.* **2017**, *40*, 351–359. [CrossRef]
65. Ezealigo, U.S.; Ezealigo, B.N.; Aisida, S.O.; Ezema, F.I. Iron oxide nanoparticles in biological systems: Antibacterial and toxicology perspective. *JCIS Open* **2021**, *4*, 100027. [CrossRef]
66. Olga, M.; Jana, M.; Anna, M.; Irena, K.; Jan, M.; Alena, Č. Antimicrobial properties and applications of metal nanoparticles biosynthesized by green methods. *Biotechnol. Adv.* **2022**, *58*, 107905.
67. El-Saadony, M.T.; Sitohy, M.Z.; Ramadan, M.F.; Saad, A.M. Green nanotechnology for preserving and enriching yogurt with biologically available iron (II). *Innov. Food Sci. Emerg. Technol.* **2021**, *69*, 102645. [CrossRef]
68. Bhat, J.A.; Bhat, M.A.; Abdalmegeed, D.; Yu, D.; Chen, J.; Bajguz, A.; Ahmad, A.; Ahmad, P. Newly-synthesized iron-oxide nanoparticles showed synergetic effect with citric acid for alleviating arsenic phytotoxicity in soybean. *Environ. Pollut.* **2022**, *295*, 118693. [CrossRef]
69. Noor, R.; Yasmin, H.; Ilyas, N.; Nosheen, A.; Hassan, M.N.; Mumtaz, S.; Khan, N.; Ahmad, A.; Ahmad, P. Comparative analysis of iron oxide nanoparticles synthesized from ginger (Zingiber officinale) and cumin seeds (Cuminum cyminum) to induce resistance in wheat against drought stress. *Chemosphere* **2022**, *292*, 133201. [CrossRef]
70. Periakaruppan, R.; Li, J.; Mei, H.; Yu, Y.; Hu, S.; Chen, X.; Li, X.; Guo, G. Agro-waste mediated biopolymer for production of biogenic nano iron oxide with superparamagnetic power and antioxidant strength. *J. Clean. Prod.* **2021**, *311*, 127512. [CrossRef]
71. Naz, S.; Islam, M.; Tabassum, S.; Fernandes, N.F.; Carcache de Blanco, E.J.; Zia, M. Green synthesis of hematite (α-Fe_2O_3) nanoparticles using Rhus punjabensis extract and their biomedical prospect in pathogenic diseases and cancer. *J. Mol. Struct.* **2019**, *1185*, 1–7. [CrossRef]
72. Zhang, W.; Rittmann, B.; Chen, Y. Size Effects on Adsorption of Hematite Nanoparticles on *E. coli* cells. *Environ. Sci. Technol.* **2011**, *45*, 2172–2178. [CrossRef]
73. Rahmani, M.B.; Ghasemi, E.; Rezaii, F. Synthesis of Wormlike α-Fe2O3 Nanostructure: Characteri-zation and Antibacterial Application. *J. Electron. Mater.* **2020**, *49*, 6087–6095. [CrossRef]
74. Annamalai, J.; Ummalyma, S.B.; Pandey, A.; Bhaskar, T. Recent trends in microbial nanoparticle synthesis and potential application in environmental technology: A comprehensive review. *Environ. Sci. Pollut. Res.* **2021**, *28*, 49362–49382. [CrossRef]
75. Tran, N.; Mir, A.; Mallik, D.; Sinha, A.; Nayar, S.; Webster, T.J. Bactericidal effect of iron oxide nanoparticles on Staphylococcus aureus. *Int. J. Nanomed.* **2010**, *5*, 277–283. [CrossRef]
76. Azam, A.; Ahmed, A.S.; Oves, M.; Khan, M.S.; Habib, S.S.; Memic, A. Antimicrobial activity of metal oxide nanoparticles against Gram-positive and Gram-negative bacteria: A comparative study. *Int. J. Nanomed.* **2012**, *7*, 6003–6009. [CrossRef] [PubMed]
77. Kohanski, M.A.; Dwyer, D.J.; Hayete, B.; Lawrence, C.A.; Collins, J.J. A common mechanism of cellular death induced by bactericidal antibiotics. *Cell* **2007**, *130*, 797–810. [CrossRef] [PubMed]
78. Sies, H. Oxidative stress: Oxidants and antioxidants. *Exp. Physiol. Transl. Integr.* **1997**, *82*, 291–295. [CrossRef]
79. Lee, C.; Kim, J.Y.; Lee, W.I.; Nelson, K.L.; Yoon, J.; Sedlak, D.L. Bactericidal effect of zero-valent iron nanoparticles on Escherichia coli. *Environ. Sci. Technol.* **2008**, *42*, 4927–4933. [CrossRef]
80. Xie, Y.; He, Y.; Irwin, P.L.; Jin, T.; Shi, X. Antibacterial activity and mechanism of action of zinc oxide nanoparticles against Campylobacter jejuni. *Appl. Environ. Microbiol.* **2011**, *77*, 2325–2331. [CrossRef]
81. Khan, A.; Roy, A.; Bhasin, S.; Emran, T.B.; Khusro, A.; Eftekhari, A.; Moradi, O.; Rokni, H.; Karimi, F. Nanomaterials: An alternative source for biodegradation of toxic dyes. *Food Chem. Toxicol.* **2022**, *164*, 112996. [CrossRef]
82. Fouda, A.; Hassan, S.E.-D.; Saied, E.; Hamza, M.F. Photocatalytic degradation of real textile and tannery effluent using biosynthesized magnesium oxide nanoparticles (MgO-NPs), heavy metal adsorption, phytotoxicity, and antimicrobial activity. *J. Environ. Chem. Eng.* **2021**, *9*, 105346. [CrossRef]
83. Saad, M.; Tahir, H.; Khan, J.; Hameed, U.; Saud, A. Synthesis of polyaniline nanoparticles and their application for the removal of Crystal Violet dye by ultrasonicated adsorption process based on Response Surface Methodology. *Ultrason. Sonochem.* **2017**, *34*, 600–608. [CrossRef]
84. Rufus, A.; Sreeju, N.; Philip, D. Size tunable biosynthesis and luminescence quenching of nanostructured hematite (α-Fe_2O_3) for catalytic degradation of organic pollutants. *J. Phys. Chem. Solids* **2019**, *124*, 221–234. [CrossRef]
85. Popov, N.; Ristić, M.; Bošković, M.; Perović, M.; Musić, S.; Stanković, D.; Krehula, S. Influence of Sn doping on the structural, magnetic, optical and photocatalytic properties of hematite (α-Fe_2O_3) nanoparticles. *J. Phys. Chem. Solids* **2022**, *161*, 110372. [CrossRef]
86. Jain, A.; Wadhawan, S.; Mehta, S. Biogenic synthesis of non-toxic iron oxide NPs via Syzygium aromaticum for the removal of methylene blue. *Environ. Nanotechnol. Monit. Manag.* **2021**, *16*, 100464. [CrossRef]
87. Routoula, E.; Patwardhan, S.V. Degradation of anthraquinone dyes from effluents: A review focusing on enzymatic dye degradation with industrial potential. *Environ. Sci. Technol.* **2020**, *54*, 647–664. [CrossRef] [PubMed]

RETRACTED

88. Bibi, I.; Nazar, N.; Ata, S.; Sultan, M.; Ali, A.; Abbas, A.; Jilani, K.; Kamal, S.; Sarim, F.M.; Khan, M.I.; et al. Green synthesis of iron oxide nanoparticles using pomegranate seeds extract and photocatalytic activity evaluation for the degradation of textile dye. *J. Mater. Res. Technol.* **2019**, *8*, 6115–6124. [CrossRef]
89. Bezbaruah, A.N.; Krajangpan, S.; Chisholm, B.J.; Khan, E.; Elorza Bermudez, J.J. Entrapment of iron nanoparticles in calcium alginate beads for groundwater remediation applications. *J. Hazard. Mater.* **2009**, *166*, 1339–1343. [CrossRef]
90. Meenachi, S.; Kandasamy, S. Investigation of tannery liming waste water using green synthesised iron oxide nano particles. *Int. J. Environ. Anal. Chem.* **2019**, *99*, 1286–1297.
91. Qureshi, K.; Ahmad, M.Z.; Bhatti, I.A.; Zahid, M.; Nisar, J.; Iqbal, M. Graphene oxide decorated $ZnWO_4$ architecture synthesis, characterization and photocatalytic activity evaluation. *J. Mol. Liq.* **2019**, *285*, 778–789. [CrossRef]
92. El-Naggar, M.E.; Shoueir, K. Recent advances in polymer/metal/metal oxide hybrid nanostructures for catalytic applications: A review. *J. Environ. Chem. Eng.* **2020**, *8*, 104175.
93. Li, Z.; Chen, Z.; Zhu, Q.; Song, J.; Li, S.; Liu, X. Improved performance of immobilized laccase on Fe_3O_4@C-Cu^{2+} nanoparticles and its application for biodegradation of dyes. *J. Hazard. Mater.* **2020**, *399*, 123088. [CrossRef]
94. Chiarello, L.M.; Mittersteiner, M.; de Jesus, P.C.; Andreaus, J.; Barcellos, I.O. Reuse of enzymatically treated reactive dyeing baths: Evaluation of the number of reuse cycles. *J. Clean. Prod.* **2020**, *267*, 122033. [CrossRef]
95. Xu, X.; Yu, J.; Liu, C.; Yang, G.; Shi, L.; Zhuang, X. Xanthated chitosan/cellulose sponges for the efficient removal of anionic and cationic dyes. *React. Funct. Polym.* **2021**, *160*, 104840. [CrossRef]

RETRACTED